FRACTAL ANALYSIS OF SURFACE MICROTOPOGRAPHY AND ITS APPLICATION IN UNDERSTANDING HYDROLOGIC PROCESSES

Y. Chi, J. Yang, D. Bogart, X. Chu

ABSTRACT. *Fractal analysis provides a useful way to characterize the spatial complexity of surface microtopography. In this study, six random roughness soil surfaces and two field plot surfaces were created. Anisotropic properties of these surfaces were examined by using the directional semivariogram method and a modified anisotropy index (a). Multifractal analysis was performed to identify the dissimilar changing patterns of fractal dimension (D) and crossover length (l) for these surfaces at different scales. It has been found that D and l at smaller scales describe topographic surfaces in more detail, while the overall topographic features of the surfaces can be captured by D and l at larger scales. Surface slope removal has a considerable effect on the fractal calculation using the semivariogram method. This study also demonstrates that fractal parameters D and l have clear and meaningful relationships with some hydrotopographic parameters, such as random roughness (RR), maximum depression storage (MDS), and number of connected areas (NCA). More importantly, fractal and anisotropic analyses enable better understanding of the overland flow generation process. A surface with a small D value has the potential to retain more water in its depressions, which in turn redistributes surface runoff water, enhances infiltration in depressions, and delays surface runoff initiation. The dominant roughness exists along the directions of smaller D values. Along those directions, surface runoff is prone to be hindered or blocked by ridges, while better hydrologic connections occur along other directions.*

Keywords. *Directional semivariogram, Hydrologic processes, Microtopography, Multifractal analysis, Overland flow generation, Surface anisotropy.*

Land surfaces are generally not smooth and exhibit spatial irregularity. The complexity of topographic surfaces relates to the smoothness of a spatial pattern, which is one of the intrinsic properties of the surface. This property has a significant influence on the behaviors of the hydrologic and geomorphologic systems (Western et al., 2001), such as overland flow generation, infiltration, and sediment transport processes. Thus, topographic analysis is fundamental to understand the mechanisms of these dynamic processes.

Fractal analysis has been widely used to characterize the spatial complexity of land surfaces (Mark and Aronson, 1984; Klinkenberg and Goodchild, 1992; Quattrochi et al., 1997; Huang, 1998; Vázquez et al., 2005, 2007). Theoretically, a surface can be considered as statistically self-similar when enlargements of any subsets of the surface have a statistical distribution identical to that of the whole surface (Feder, 1988). In practice, self-similarity can be determined by evaluating the linearity of the best-fit curve of semivariogram [$\gamma(h)$] and lag distance (h) on the log-log plot during the calculation of fractal dimension (D) using the semivariogram method (Yokoya et al., 1989; Klinkenberg and Goodchild, 1992). If the curve is approximately linear for all lags, the surface is consistent with the concept of self-similarity (Mark and Aronson, 1984), and monofractal analysis can be applied. In reality, however, such a surface rarely exists. Most surfaces may show partially self-similar, so a fractal model can be applied only within a limited range or distance (Mark and Aronson, 1984; Yokoya et al., 1989; Xia, 1993; Huang, 1998; Vázquez et al., 2007; Abedini and Shaghaghian, 2009). Out of the range, different D values may exist for the surfaces (Mark and Aronson, 1984). Thus, many studies were conducted to examine the multifractal property of surface topography, which involved identification of breakpoints and determination of multiple linear segments and the corresponding D values (e.g., Mark and Aronson, 1984; Klinkenberg, 1988; Lovejoy et al., 1995; Gagnon et al., 2006; Abedini and Shaghaghian, 2009). Mark and Aronson (1984) found that most of their selected geographic surfaces showed varying D values at different scales. The D values derived from the middle scale were always greater than those from the smaller scale.

D is one of the major fractal parameters. Fractal D of a surface represents its capability to "fill" the space in which it resides (Abedini and Shaghaghian, 2009). Thus, the more a surface fills the space, the higher D it has (Sun et al., 2006). Surfaces with higher D values appear more disordered or display a rapid succession of peaks and valleys in a short distance, but show smaller variability at a large dis-

Submitted for review in March 2012 as manuscript number SW 9691; approved for publication by the Soil & Water Division of ASABE in September 2012.

The authors are **Yaping Chi,** Graduate Student, **Jun Yang,** Graduate Student, **Daniel Bogart,** Graduate Student, and **Xuefeng Chu,** Assistant Professor, Department of Civil Engineering, North Dakota State University, Fargo, North Dakota. **Corresponding author:** Xuefeng Chu, Department of Civil Engineering (Dept. 2470), North Dakota State University, P.O. Box 6050, Fargo, ND 58108-6050; phone: 701-231-9758; e-mail: xuefeng.chu@ndsu.edu.

  ISSN 2151-0032

tance (Sung et al., 1998). However, surfaces with lower D values have greater variations in elevation (e.g., larger and deeper depressions), and thus more space is left "unfilled." Based on fractal analysis of some agricultural soil surfaces, Huang (1998) concluded that a relatively lower D value of a surface indicated a higher contrast of aggregates/clods on the surface, while a higher D value denoted overall gradual changes in surface elevations. It has been observed that a surface with a D value greater than 2.5 implies a negative spatial autocorrelation between two points at the scale where D is derived (Burrough, 1983; McClean and Evans, 2000). Thus, detailed topographic information may be lost at a sampling interval larger than that scale. In contrast, surfaces with a D value smaller than 2.5 are less rugged and show positive spatial autocorrelation within the scale associated with the D (Burrough, 1983). The semivariogram method has been widely accepted to calculate D (Klinkenberg and Goodchild, 1992; Xia, 1993). In the application of the semivariogram method for fractal analysis, however, it is critical to determine the breakpoint distances (d_B) to find the best-fit linear regression lines of the semivariogram curve at different scales in the calculation of D.

D may not be a unique parameter for characterizing surface topography. Two surfaces of dissimilar topographic features may have the same D value (Klinkenberg, 1988; Huang and Bradford, 1992). Together with D, the ordinate intercept (I_c) of the best-fit linear segment of the semivariogram curve also has been used to characterize surface topography (Klinkenberg and Goodchild, 1992; Abedini and Shaghaghian, 2009). Alternatively, crossover length (l), which is derived from I_c, is often combined with D to characterize soil surface microrelief (Huang and Bradford, 1992; Vázquez et al., 2005, 2007). D represents the horizontal variability in surface roughness with scale, while I_c or l reveals the degree of vertical topographic variations at a reference scale (Klinkenberg, 1988; Klinkenberg and Goodchild, 1992; Huang and Bradford, 1992; Vázquez et al., 2007). For the same scale, a rougher surface has a greater l value (Eltz and Norton, 1997).

One of the major advantages of the semivariogram method for fractal analysis is that it can quantify directional variability (i.e., anisotropy) of surface topography (Xia, 1993; Vázquez et al., 2005). Vázquez et al. (2005) applied the semivariogram method to capture the tillage direction of agricultural fields since the D value is much higher along the tillage direction. Klinkenberg (1988) calculated angular variograms to quantify surface anisotropy and detect the dominant directions of surface roughness.

In the applications of the semivariogram method, any data trend (e.g., slope) should be removed to satisfy the major assumption introduced in this method (Perfect and Kay, 1995). However, Armstrong (1986) found that removal of periodic components had no substantial effect on the computation of the semivariogram, and hence the D value. Abedini and Shaghaghian (2009) also found that surface detrending methods (e.g., linear, quadratic, and cubic fitting plane methods) had a minimal effect on D. Armstrong (1986) and Klinkenberg and Goodchild (1992) suggested that for fractal analysis of land surfaces, it is not necessary to remove the non-stationarity of the data in the semivariogram calculation since surface slope is a part of the topographic properties. However, Vázquez et al. (2010) removed the slope of soil surface microrelief by finding a best fitting plane (linear, quadratic, or cubic fitting plane), and concluded that trend removal did affect the fractal indices (D and l). Thus, further studies are needed to evaluate the effect of surface trend removal on fractal analysis.

In addition to the fractal method, the random roughness (RR) index (Allmaras et al., 1966) has been widely used to quantify soil surface roughness (Govers et al., 2000; Kamphorst et al., 2000), especially for agricultural fields. Along with RR, the maximum depression storage (MDS) is another important hydrotopographic parameter that represents the capacity of a topographic surface in storing water in depressions. Depressions are one of the most important topographic features. Many studies have demonstrated the great effect of surface depressions on surface runoff (e.g., Martin et al., 2008). Surface depressions tend to delay the initiation of surface runoff (Darboux and Huang, 2005) and retain more surface runoff water (Abedini et al., 2006). Particularly, surface runoff occurs before all depressions are fully filled (Moore and Larson, 1979; Onstad, 1984; Darboux et al., 2001). Darboux and Huang (2005) also found that as rainfall accumulates, more depressions of a surface become well connected so that more runoff water contributes to the outlet discharge. In other words, hydrologic connectivity of the surface is enhanced. Depressions affect the spatial distributions of water on a land surface by storing water, and thus dominate the overall connectivity of the topographic surface and break the surface into a number of well connected areas (CAs) that have independent and localized hydrologic mass balance (Hayashi et al., 2003). Each localized CA consists of a depression and its contributing area. Thus, the number of CAs (NCA) can represent the complexity of surface microtopography. A higher NCA indicates stronger irregularity in surface topography (i.e., more depressions/puddles). Thus, the NCA can be used to help understand overland flow process on rough surfaces. Now that the fractal parameters (D and l), RR, MDS, and NCA all can be used to characterize surface microtopography, it is of importance to examine their relationships, which will further improve the understanding of the effects of surface microtopography on hydrologic processes.

In this study, surface microtopography is characterized by fractal analysis and three hydrotopographic parameters (RR, MDS, and NCA). The relationships of these hydrotopographic parameters with the fractal parameters D and l are examined. The effect of surface slope removal on fractal analysis is evaluated. In addition, the anisotropic properties of surface roughness are analyzed by using the directional semivariogram method and a modified anisotropic index, and dominant roughness directions are identified. Most importantly, efforts are made in this study to investigate the possibility to use the fractal parameters D and l and the anisotropy analysis results to improve the understanding of the overland flow generation process.

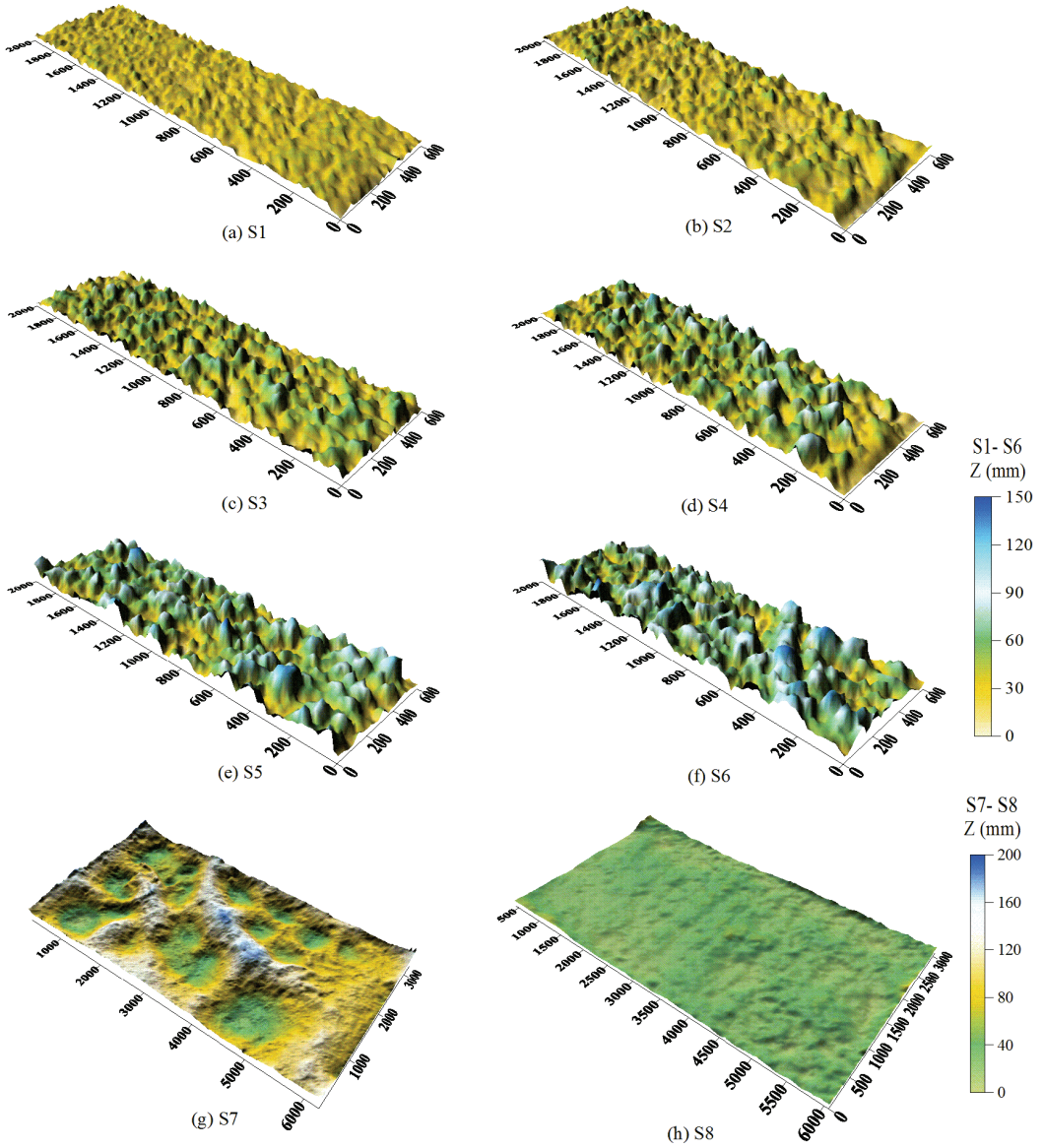

Figure 1. Six laboratory surfaces (S1 to S6) and two field plot surfaces (S7 and S8).

Materials and Methods

Surface Data

Six laboratory soil surfaces (S1 to S6) and two field plot surfaces (S7 and S8) were created (fig. 1). The laboratory surfaces S1 to S6 (figs. 1a to 1f) were created by randomly distributing soil aggregates (i.e., no oriented roughness) across a flat area. Thus, the overall slopes of the surfaces were zero. The aggregates were collected in the field without vegetation. The sizes of major soil aggregates increased gradually from S1 to S6. The area of S1 to S6 was 0.6 m × 2.0 m. The field plot surfaces S7 and S8 (figs. 1g and 1h) were constructed at the main station of the North Dakota Agricultural Experiment Station (NDAES) in Fargo, North Dakota. Both plots had an area of 6.0 m × 3.2 m and an overall slope of 2.5% towards their outlets. Surfaces S7 and S8 respectively represented rough and smooth field surfaces. The rough surface (S7) featured a number of depressions and mounds, while the smooth surface (S8) was essentially an inclined plane with minimal topographic variations. Both the laboratory and field surfaces were scanned by using an instantaneous-profile laser scanner (Darboux and Huang, 2003). The vertical and horizontal resolutions of the scanned DEMs were 0.5 mm and 0.98 mm, respectively. The scanned data were further processed to generate the DEMs with horizontal resolutions of 10 mm and 20 mm for S1-S6 and S7-S8, respectively. Surface S8 was used for evaluating the effect of slope removal on the computation of the semivariogram and consequently D and l. The anisotropic properties of surfaces S1 to S8 were analyzed to identify the dominant roughness directions. Moreover, surfaces S1 to S6 were utilized to examine the relationships between D and RR, MDS, and NCA, and these relationships were further used to interpret how surface microtopography affected the overland flow process on rough surfaces.

Calculation of Fractal Dimension *D*

As aforementioned, the semivariogram method was used

to calculate fractal parameters in this study. Based on the DEM data, the semivariogram is given by:

$$\gamma(\mathbf{h}) = \frac{1}{2N(\mathbf{h})} \sum_{i=1}^{N(\mathbf{h})} [Z(\mathbf{s}_i + \mathbf{h}) - Z(\mathbf{s}_i)]^2 \quad (1)$$

where $\gamma(\mathbf{h})$ is the semivariogram, $\mathbf{s}_i$ is location i, $\mathbf{h}$ is the lag distance, $Z(\mathbf{s}_i)$ is the elevation at location $\mathbf{s}_i$, $Z(\mathbf{s}_i + \mathbf{h})$ is the elevation at location $(\mathbf{s}_i + \mathbf{h})$, and $N(\mathbf{h})$ is the number of pairs spaced at $\mathbf{h}$.

Based on the calculated semivariogram $\gamma(\mathbf{h})$, D and I_c can be determined. For a fractal Brownian motion (fBm) model, the elevation change $\Delta Z(h)$ and the structural function are respectively given by (Huang and Bradford, 1992):

$$\Delta Z(h) \propto h^H \quad (0 < H < 1) \quad (2)$$

and

$$\gamma(h) \propto h^{2H} \quad (3)$$

where H is the Hurst exponent, and $\Delta Z(h)$ is the difference in elevations at distance h. Thus, the semivariogram $\gamma(h)$ can be expressed as:

$$\gamma(h) = Kh^{2H} \quad (4)$$

or

$$\log[\gamma(h)] = 2H\log(h) + \log(K) \quad (5)$$

where K is the proportional factor. Equation 5 shows a linear relationship between $\log[\gamma(h)]$ and $\log(h)$ with a slope (S) of $2H$ and an intercept (I_c) of $\log(K)$. That is, $H = S/2$. Given the Hurst exponent H, the fractal dimension D of a topographic surface (Euclidean dimension $d = 3$) is given by:

$$D = 3 - H = 3 - 0.5S \quad (6)$$

Following Huang and Bradford (1992), K in equation 4 can be expressed as a function of crossover length l:

$$K = l^{2-2H} \quad (7)$$

Thus, crossover length l can be determined by K and H from the best-fit linear line of the log-log semivariogram curve. Figure 2 schematically shows the procedures for determining D, I_c, and d_B by using the semivariogram method. As aforementioned, the key step to calculate D is to find the best-fit linear segment of the semivariogram curve. Since more than one linear segment of the semivariogram may exist for some surfaces, multiple linear lines can be fitted to the corresponding linear segments, if applicable, to analyze the fractal properties of the surfaces at different scales. The breakpoints are determined based on the distribution of $\gamma(h)$ and h on the log-log plot. The linear segment of the log-log semivariogram curve (eq. 5) is then fitted by using the least-square regression method. The goodness of the least-square regression can be evaluated by:

$$R^2 = 1 - \frac{\sum_{i=1}^{n} (\gamma_i - \hat{\gamma}_i)^2}{\sum_{i=1}^{n} (\gamma_i - \bar{\gamma})^2} \quad (8)$$

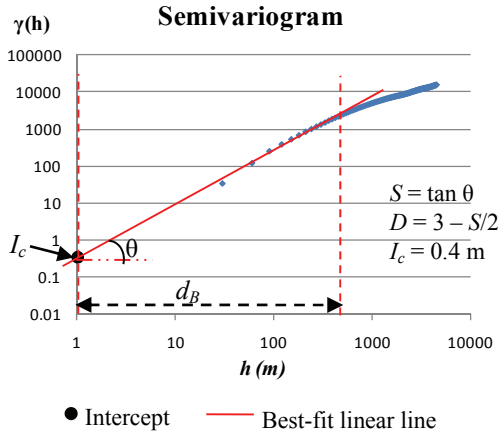

Figure 2. Determination of fractal dimension D, ordinate intercept I_c, and breakpoint distance d_B.

where R^2 is the coefficient of determination, γ_i is the actual semivariogram at ith distance, $\hat{\gamma}_i$ is the estimated semivariogram at ith distance, $\bar{\gamma}$ is the average value of the actual semivariogram for all distances, and n is the total number of lag distances h for semivariogram calculation. A Windows-based fractal analysis program has been developed by using C# to facilitate the computations of $\gamma(h)$, D, and I_c. The coordinate system is set so that angles are described as follows: 0° is defined as east and angles proceed in a counter-clockwise direction where 180° is west and 360° returns to the east direction.

Calculations of RR, MDS, and CAs

Chu et al. (2012) examined different procedures for computation of RR using the method developed by Allmaras et al. (1966). They found that the procedures of slope removal and removal of the upper and lower extreme DEM data points were necessary for the computation of RR. Thus, the program from Chu et al. (2012) was used to calculate RR values for the six random rough surfaces (S1 to S6). Based on the DEM of each surface, the puddle delineation (PD) software (Chu et al., 2010; Chu, 2011) was utilized to identify puddles and their relationships, determine flow directions based on the D8 method (O'Callaghan and Mark 1984) and flow accumulations, and compute the MDS of the surface. In addition, the CAs and NCA were determined through a searching process in the PD program, which identified all hydrologically connected cells.

In this study, we quantified the relationships between fractal D and the hydrotopographic parameters RR, MDS, and CA for surfaces S1 to S6. These relationships "bridged" the gap between fractal analysis and hydrologic analysis and linked fractal parameters D and l to certain hydrologic processes (e.g., overland flow generation).

Effect of Surface Slope Removal

Surface S8 was used to evaluate the effects of surface slope on the calculation of fractal parameters (D and l). The surface slope was removed by finding a best-fit plane (linear, quadratic, or cubic fitting plane). Then the effect of surface detrending on fractal analysis was evaluated by comparing the fractal parameters (including D and l) of the

surfaces with and without slope removal.

Anisotropy of Surface Microtopography

Anisotropic properties of surface microtopography were analyzed for the eight surfaces (fig. 1). Besides omni-directional semivariograms, directional semivariograms were calculated for angles from 0° to 360° with an interval of 15° for these surfaces. D and l were then determined for all directions and plotted in the rose plot to show their directional distributions. In addition, an anisotropy index (a) was calculated to further quantify the anisotropic/isotropic properties of surface topography. This index was modified from Green and Erskine (2004) as follows:

$$a = 10^{\mathrm{SD}(D)} \tag{9}$$

where SD(D) is the standard deviation of D values along the 24 directions. The power function of 10 was introduced to magnify the index since the SD(D) was usually very small. Theoretically, a equals 1 for a perfect isotropic surface and increases with the degree of anisotropy.

Overland Flow Experiment

The overland flow experiment, which was used for evaluating the influence of surface microtopography on overland flow generation in this study, was conducted on the rough and smooth field plots (S7 and S8) under natural rainfall on August 12, 2011. After scanning the two field plot surfaces using the laser scanner, they were covered by large tarps to protect the surfaces and minimize soil moisture changes during dry periods. At the base of each plot, an outlet collection structure was built. Runoff naturally flowed towards the outlet due to the overall slope and was concentrated using tapered metal sheeting that led to a collection spout consisting of gutter and PVC piping. The runoff was then deposited into a volumetric measuring device. During the experiment, the volume of runoff was observed and recorded at set time intervals. The measured discharge data allowed for the hydrographs of the rough and smooth surfaces under the same rain event to be compared. Additionally, a tipping-bucket rain gauge (HOBO data logging rain gauge RG3, Onset Computer Corp., Bourne, Mass.) was installed to measure rainfall, and soil moisture sensors were installed to record soil moisture contents in both plots. Hydrologic analysis was performed using the rainfall, runoff, and soil moisture data collected in the field and the surface depression storage calculated from the DEMs.

Results and Discussions

Surface Detrending Effect on Fractal Analysis

Field surface S8 (fig. 1h) was selected for evaluating the surface detrending effect on fractal analysis. For S8, the best-fit plane was a cubic one ($R^2 = 0.999$). Figure 3 shows the comparison of omni-directional semivariogram curves of the surfaces with and without surface detrending. It can be observed that surface slope significantly affects the computation of the semivariogram (fig. 3). For a sloping surface without slope removal, the semivariogram increases continuously with increasing h due to the overall slope-related increase in elevations. After slope removal, the semivariogram reaches a sill beyond the distance of about 700 mm (fig. 3). Although the semivariogram may be similar within a short distance, it changes significantly for a larger h after surface slope removal or detrending (fig. 3). The differences in the semivariograms imply that significant changes in fractal parameters D and l are expected. The scale (i.e., d_B) at which D is determined also varies accordingly. Table 1 shows the D and l values calculated for surfaces with and without detrending or slope removal. It can be observed that the breakpoint distance (i.e., d_B) at which D and l were derived changes from 1341 mm without detrending to 320 mm with detrending; the relative difference in D is 2.88%, while the relative difference in l reaches up to 100%, indicating that l is more sensitive to the slope removal.

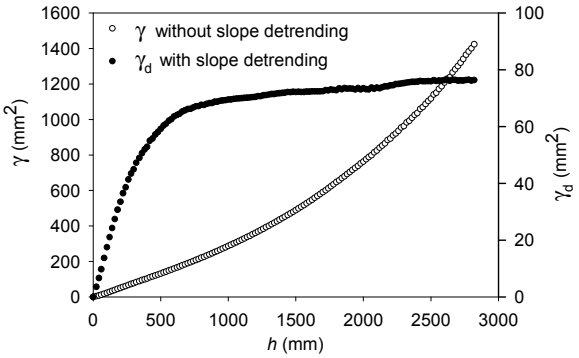

Figure 3. Comparison of omni-directional semivariograms for surface S8 with and without surface detrending.

Table 1. Fractal dimension (D), crossover length (l), and breakpoint distance (d_B) values for surface S8 with and without surface trend removal.

	D	l (mm)	d_B (mm)
Without detrending	2.43	0.1	1,341
With detrending	2.50	0.2	320
Relative difference (%)	2.88	100	

The preceding discussions demonstrate that surface slope removal significantly changes the semivariogram calculation, and consequently affects fractal parameters D and l. Therefore, surface slope should be removed before calculating the semivariogram and applying fractal analysis to characterize surface microtopography. In this study, the overall slope for each surface was removed before analyzing surface microtopography.

Interpretation of Fractal Dimension and Crossover Length

Laboratory Surfaces

Figure 4 shows the omni-directional semivariograms for the six laboratory surfaces (S1 to S6) and the two field surfaces (S7 and S8). Both sills and ranges increase from S1 to S6 as the size of soil aggregates becomes larger (figs. 4a to 4f). For surfaces S1 to S6, the semivariograms increase rapidly for small lag distances (h), indicating a close correlation of elevation variations at that scale (h). The semivariograms then become relatively stable (sill) beyond a certain h (range), which varies slightly among surfaces (figs. 4a to

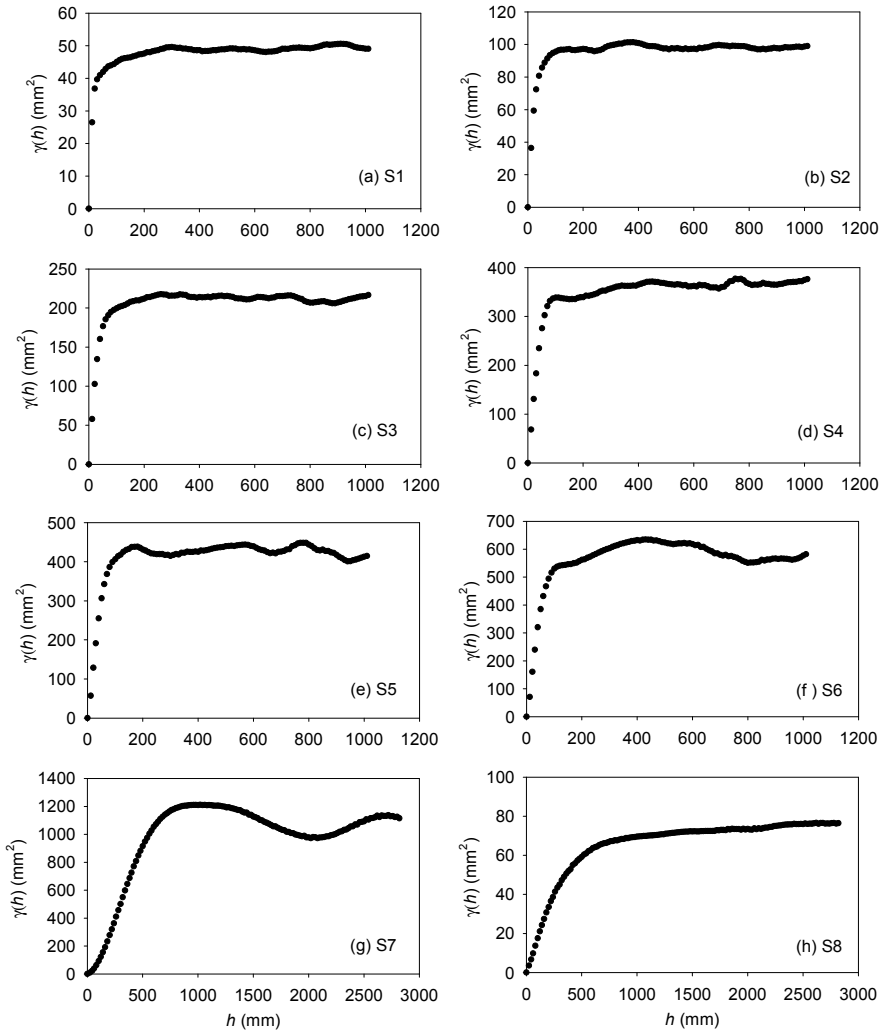

Figure 4. Omni-directional semivariogram curves for the six laboratory surfaces (S1 to S6) and two field surfaces (S7 and S8).

4f). Table 2 shows the results of omni-directional fractal parameters for S1 to S6. *D* values decrease gradually as soil aggregates become larger (table 2). Surface S1, with the smallest soil aggregates, shows rapid changes in mounds and depressions on the surface, indicating more irregularity and thus resulting in a higher *D* value. This result is consistent with the findings by Zribi et al. (2000) and Sun et al. (2006). In contrast, surface S6 with the largest soil aggregates has the lowest *D* value since the changes in elevations are more gradual and smoother at local scales. The *D* values for the six surfaces (S1 to S6) decrease from 2.95 to 2.65. The *l* values vary from 5.9 mm for S1 to 11.3 mm for S6 (table 2). A higher *l* value indicates greater variability in surface elevations at the scale where *D* is derived. Thus, a rougher soil surface has a higher *l* value. For example, in spite of the small difference in *D* values (0.05) between S2 and S3, their difference in *l* values is as high as 2.6 mm (table 2). In addition, surfaces with dissimilar topographic characteristics may have similar *D* values. Hence, *D* and *l* should be jointly used to quantify surface topographic properties; the former describes the horizontal roughness that is scale dependent, and the latter captures the vertical variability in elevations at the scale where *D* and *l* are derived.

Table 2. Random roughness (RR), maximum depression storage (MDS), number of connected areas (NCA), omni-directional fractal dimension (*D*), and crossover length (*l*) for the six laboratory surfaces.

Surface	RR (cm)	MDS (cm^3)	NCA	*D*	*l* (mm)
S1	0.44	1370.2	117	2.95	5.9
S2	0.62	1690.4	92	2.89	7.5
S3	0.89	1863.6	99	2.84	10.1
S4	1.12	2058.6	89	2.72	10.3
S5	1.29	2512.4	66	2.69	10.3
S6	1.50	3207.7	60	2.65	11.3

Field Surfaces

For both field plot surfaces S7 and S8 (figs. 1g and 1h), the semivariograms increase significantly within smaller lag distances (*h*) and then approach to their sill values (figs. 4g and 4h). However, the variance value (sill value) for S7 reaches up to about 1200 mm^2 and the sill value of S8 is only approximately 70 mm^2, which indicates that S7 exhibits much greater variations in elevation than S8 does. The semivariogram of S8 shows an asymptotic sill beyond the lag distance (*h*) of around 700 mm, implying that beyond this lag distance no spatial correlation exists. Oscillation in surface microtopography of S7 can be observed for the larger *h* part of the semivariogram curve of S7 (*h* is

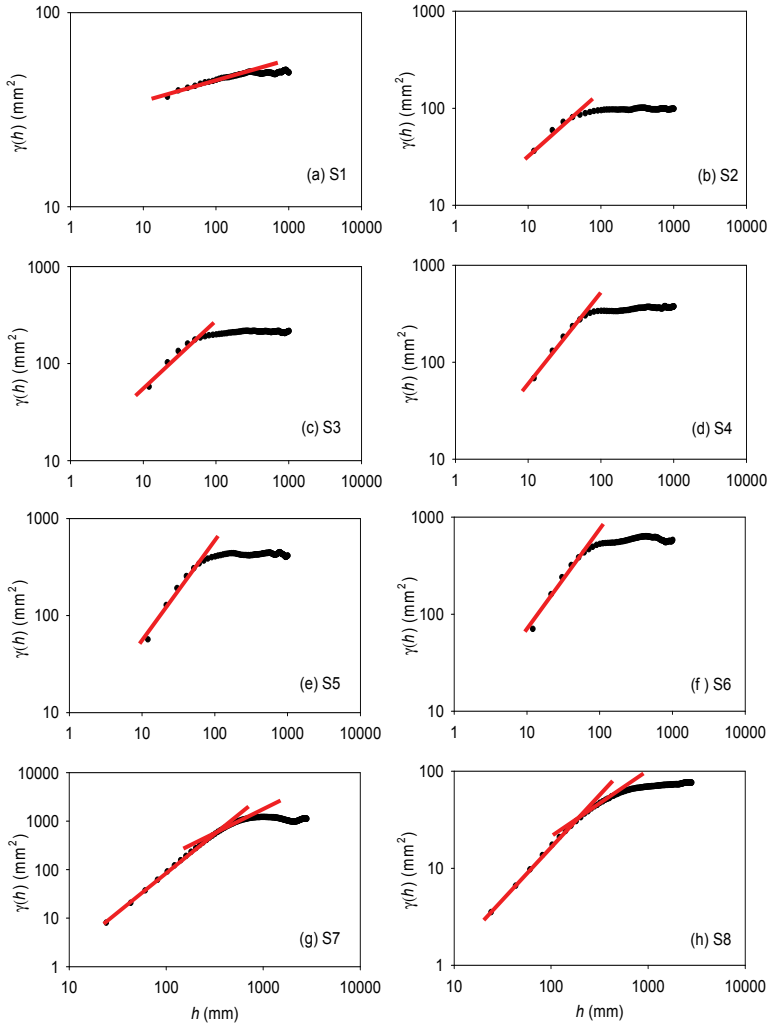

Figure 5. Omni-directional semivariogram curves and the fitted linear lines (red color) for the six laboratory surfaces (S1 to S6) and two field surfaces (S7 and S8) on a log-log scale.

greater than 1300 mm) (fig. 4g).

Figure 5 shows the omni-directional semivariograms for the eight surfaces (S1 to S8) on a log-log scale with the fitted linear lines that are used to derive the D and l. Only one linear segment is observed for each of the semivariograms of the six random roughness surfaces (S1 to S6) within certain distances. Thus, fractal analysis for these six surfaces focuses on one linear segment (figs. 5a to 5f). However, for the two field plot surfaces (S7 and S8), the semivariogram curves on the log-log plot exhibit two linear segments before reaching the sills (figs. 5g and 5h). Thus, multifractal analysis is performed for these two surfaces by fitting two linear segments on the semivariogram curves. The first linear segment characterizes the smaller scale surface topography, while the second segment reveals topographic variability on a larger scale.

Table 3 shows the omni-directional fractal parameters for surfaces S7 and S8 at the two scales. S7 has much smaller D and l values for the small scale (D = 2.20, l = 0.0005 mm, and d_B = 419.9 mm) than those for the large scale (D = 2.63, l = 2.0 mm, and d_B = 700.8 mm) (table 3). This low D value of S7 at the small scale captures the characteristics of local depressions and mounds on the surface. Note that a lower D value implies that less volume of the surface is "filled," while a higher D value suggests that the surface is almost "filled" to reach the 3D dimension. This conclusion can be verified based on the microtopographic characteristics of S7. The sizes of major depressions on S7 are larger than 400 to 500 mm in diameter (fig. 1g). Thus, within the scale of the depressions (i.e., h = 400 to 500 m), more space is less "filled," and the vertical variation of elevations is small, resulting in low D and l values. In addition, a low D value indicates that the surface is "smooth" at the corresponding scale. The elevation points within this scale are correlated so that the elevation of any point can be interpolated by its neighboring points. However, beyond this scale, the detailed information of the surface is miss-

Table 3. Omni-directional fractal parameters for surfaces S7 and S8 at two scales.

Surface	Segment	Fractal Dimension (D)	Crossover Length (l, mm)	Breakpoint Distance (d_B, mm)
S7	1st	2.20	0.0005	419.9
	2nd	2.63	2.0	700.8
S8	1st	2.50	0.2	320.1
	2nd	2.79	1.7	680.1

ing, resulting in a sharp change in the semivariogram curve. This break at the horizontal scale leads to the fractal *D* changes. But elevations may change significantly at a larger scale (a larger *h*) (Sung et al., 1998). The *D* and *l* for the second segment reveal large-scale topographic features, such as the distribution of depressions across the entire surface. The *D* and *l* values for the second segment are much greater than those for the first segment (table 3), implying that at a larger spatial scale (*h* = 419.9 to 700.8 mm) more significant changes in elevations dominate the surface topography for surface S7.

Similar results can be observed for S8. That is, *D* and *l* values from the second segment are higher than those of the first segment (table 3). The *D* value of 2.79 at the scale of 320.1 to 680.1 mm indicates that the autocovariance of surface elevations at this scale is low. In other words, the surface is relatively disordered. In spite of the overall smoothness of S8, small variations in surface elevations are random (fig. 1h). Overall, S8 has greater *D* values than S7 for both segments, indicating much more rapid local changes in surface elevations for S8 (table 3). Based on *D* and *l* values, it can be concluded that at a small scale S7 shows significant topographic variations with spatial scales along the horizontal direction (low *D*) and smaller vertical variability in elevations (low *l*) at the reference scale. Surface S8 looks smooth (high *D*), but the local variability in elevations is greater (higher *l*). Thus, multifractal analysis can be a useful way to identify the scale at which the dominant topographic characteristics of surfaces change. This critical scale is determined based on the obvious change in the semivariogram curve and the calculated *D* value.

Multifractal Analysis and Anisotropic Properties of Surface Topography

Anisotropy of microtopography was analyzed for the eight laboratory and field surfaces by using directional fractal parameters. Figure 6 shows the rose plots of *D* and *l* for surfaces S1 to S6 along the 24 selected directions. Since the *D* and *l* values for the upper portion (0° to 180°) and the lower portion (180° to 360°) are symmetrically distributed about the origin (fig. 6), discussions focus on the upper 180° portion. For surfaces S1 to S6, soil aggregates are randomly distributed, and there are no slope and oriented tillage marks (figs. 1a to 1f). Minor directional variations in *D* and *l* can be observed for all the six microtopographic soil surfaces, and especially the surfaces with smaller aggregates show certain isotropic property (fig. 6). It can be observed that for different surfaces, the rose plots of *D* and *l* display different changing patterns. Generally, *D* decreases and *l* increases from S1 to S6 as the sizes of aggregates increase (fig. 6). These decreasing or increasing patterns are consistent with the results from the omni-directional fractal parameters.

Figure 7 shows the distributions of fractal *D* and *l* for the two field surfaces S7 and S8 along the 24 selected directions at two scales. For surface S7 at the small scale (first segment), *D* captures the detailed topographic information within the local depression scale (depressions are within this scale) of the surface. The distribution of *D* values shows certain isotropy (fig. 7a). In addition, the shapes of the depressions on S7 do not have any directionally distributed patterns. However, *l* values of S7, ranging from 0.0002 mm to over 0.002 mm (fig. 7a), exhibit obvious anisotropic properties. The *l* values depict the vertical elevation changes along different directions. Even though the change in *l* seems great, the changing magnitude actually is of an order of 10^{-3} (fig. 7a). Thus, the vertical variations in surface elevations at the small scale are small. On the contrary, the *D* values of S7 at the large scale (second segment) show more anisotropic properties. The *D* values along 90° to 120° are the smallest among all directions (fig. 7b). This can be attributed to the surface microtopography of S7. Along 90° to 120°, surface microtopography exhibits more undulation because of the two major ridges across the surface, but the change in elevations is smooth and gradual (fig. 1g).

For surface S8, *D* and *l* show stronger anisotropic distributions at a small scale and more uniform distributions at a larger scale, which are opposite from S7 (figs. 7c and 7d).

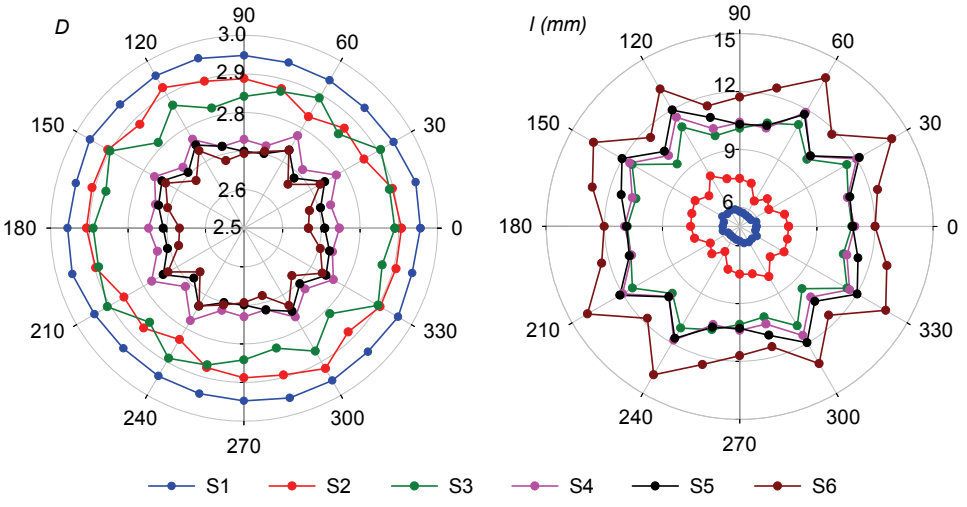

Figure 6. Distributions of fractal dimension *D* and crossover length *l* for surfaces S1 to S6 along the 24 selected directions.

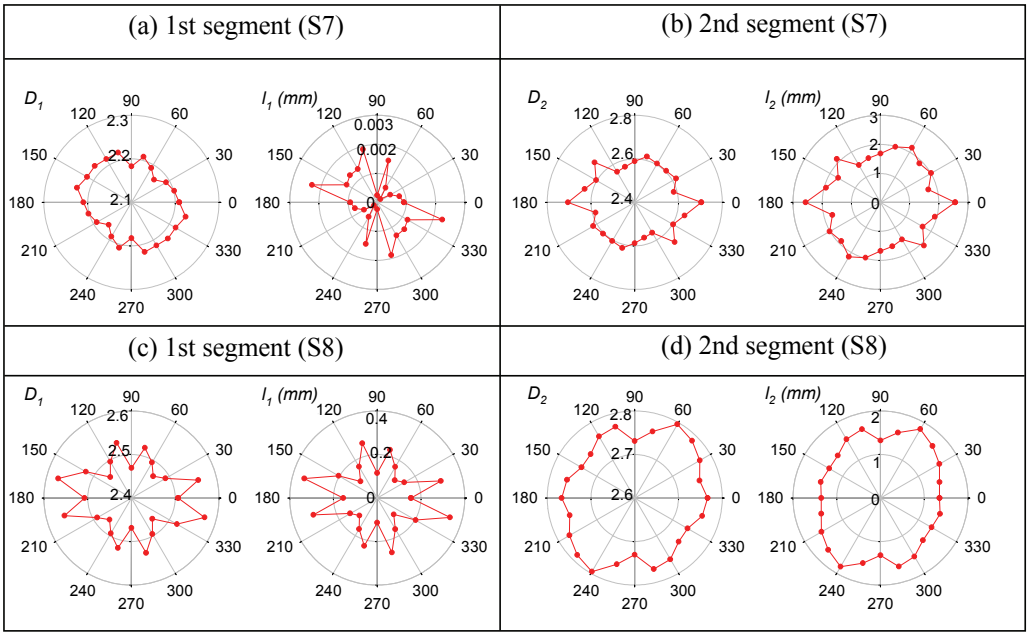

Figure 7. Distributions of fractal dimension *D* and crossover length *l* for surfaces S7 and S8 along the 24 selected directions at two scales.

For this relatively smooth surface (S8), the change in elevations at the small scale reflects the local variations associated with small aggregates. At the larger scale, the correlation between elevation points is low, and the surface looks smooth. Thus, the surface had relatively uniform distributions of *D* and *l* along all directions (fig. 7d).

It should be noted that S7 shows stronger anisotropy at a larger scale than S8 does at a smaller scale (fig. 7). This difference can be attributed to their distinct topographic features. The overall distribution of depressions across surface S7 can be captured by the anisotropically distributed *D* and *l* at the large scale, while the topographic information of each depression can be depicted at the small scale. For surface S8, the characteristic of overall smoothness can be captured by the distributions of *D* and *l* at the larger scale, while the minor variations in elevations at the small scale across the surface result in the non-uniform distributions of *D* and *l* (fig. 7). Thus, the directional fractal parameters *D* and *l* can be useful indicators for quantifying the anisotropic properties of topographic surfaces.

Table 4 shows the calculated anisotropy index (*a*) values (eq. 9) for the eight surfaces. Basically, the *a* values for the six laboratory surfaces (S1 to S6) are very close except for S1 (table 4). S1 has the lowest *a* value, indicating that the surface with small aggregates possesses good isotropic properties. As to the field plot surfaces, S7 and S8 show strong anisotropy with higher *a* values at the large and small scales, respectively (table 4). These findings are in accordance with those from the rose plots showing the directional distributions of *D* in figures 4 and 5. Thus, the anisotropy index *a* can be effectively used to quantify the anisotropic property of surface microtopography.

Relationships of Fractal and Hydrotopographic Parameters

Table 2 shows the calculated fractal parameters *D* and *l*, and the hydrotopographic parameters RR, MDS, and NCA. For surfaces S1 to S6, the *D* values decrease from 2.95 to 2.65 and the NCA values decrease from 117 to 60, except for S3 (table 2). However, the RR values increase from 0.44 to 1.50 cm, the *l* values increase from 5.9 to 11.3 mm, and the MDS values increase from 1,370 to 3,208 cm^3 from S1 to S6 as their soil aggregates become larger (table 2). Generally, a random rough surface with a greater *D* value (e.g., S1) has smaller RR and MDS values and a higher NCA value. That is, such a surface (S1) is relatively smooth (low RR), has shallow and small depressions/puddles (low MDS), and consists of a considerable number of isolated areas (high NCA). However, a surface with a smaller *D* value (e.g., S6) has greater variations in surface elevations (high RR), deeper and larger depressions/puddles (high MDS), and fewer isolated areas (low NCA). These dissimilar topographic characteristics of the surfaces affect their responses to a rainfall event. For a surface of a greater *D* (e.g., S1), the puddle filling and spilling processes occur more frequently and quickly, the isolated areas more easily connect or merge with each other, and the overland flow system more easily reaches a steady state. Since both RR and *l* represent the vertical elevation variations, similar changing patterns of RR and *l* are expected. Thus, only the relationship between *D* and RR is examined in this study.

In summary, a rougher soil surface of a smaller *D* value has a higher RR, which results in a greater MDS (Chu et al., 2012). This implies that *D* and MDS are negatively correlated. NCA depends on the number of depressions/puddles on the surface. A complex surface that con-

Table 4. Anisotropy index for the six laboratory surfaces (S1 to S6) and the two field surfaces (S7 and S8).

							S7		S8	
	S1	S2	S3	S4	S5	S6	1st Segment	2nd Segment	1st Segment	2nd Segment
Anisotropy index (*a*)	1.01	1.06	1.07	1.05	1.05	1.06	1.04	1.09	1.08	1.04

sists of more puddles has a higher *D* value. The hydrotopographic parameters RR, MDS, and NCA characterize surface microtopography and the relevant hydrologic properties, and the fractal parameters *D* and *l* provide more complementary information related to topographic variability and scale-dependent processes. The relationships between the hydrotopographic and fractal parameters allow application of fractal *D* and *l* to analyze the related hydrologic processes, as detailed in the following section. It should be noted, however, that a fractal index cannot be directly used to calculate MDS (Kamphorst et al., 2000).

Fractal Analysis versus Overland Flow Processes under the Influence of Surface Microtopography

The behaviors of the hydrologic system are influenced by the formation and evolution process of the connected areas or the sub-drainage systems. In a rainfall-runoff event, each of the CAs initially has its own drainage system and independent mass balance. With a continuous rainfall input, runoff water flows from cell to cell along the elevation gradient and accumulates in the related puddles. The water level in such a puddle gradually increases until it reaches the threshold of the puddle. Then the rainfall excess spills to a downstream puddle. Two or more CAs also can be merged to form a bigger CA, which enables the CAs to be connected hydrologically. Consequently, stepwise increases in discharge at the outlets are expected. The formation and evolution of the CAs and the related hydrologic processes are highly dynamic in temporal and, in particular, spatial distributions, depending on the inputs of the hydrologic system (e.g., rainfall characteristics) and the properties of the hydrologic system (e.g., surface topography, soil properties, initial moisture condition, etc.).

Figure 8 shows the overland flow experiments conducted on surfaces S7 and S8. Due to the clay-textured soil (0% sand, 17.5% silt, and 82.5% clay), the moisture content for any sensor changed only 4% or less during the experiment period. These relatively insignificant changes in the soil moisture conditions allowed for simplification in the comparison of surface runoff for the two plots. Overall, the soil maintained a high moisture content level throughout the experiment period. Thus, the distributions of water on the surfaces were primarily controlled by the topographic conditions (figs. 8a and 8b). Figure 8c shows the hyetograph combined with hydrographs for surfaces S7 and S8 for the selected rainfall event. The rainfall began with a short and low-intensity phase, followed by a brief but higher-intensity period and eventually dropping to a lower intensity with some minor variations. The effect of these variations in rainfall intensity translated well when considering the hydrograph of the smooth surface (fig. 8c). That is, the hydrograph of the smooth surface reflected the intensity variations of the hyetograph. During the high-intensity portion of the rain event, the surface runoff from S8 began with a high flow rate and subsequently dropped with the hyetograph. Beyond this point, the hydrograph of S8 rose and fell with the rainfall rate. This was particularly visible for the later rain event during the second peak in rain intensity (fig. 8c). However, the hydrograph of the rough surface (i.e., S7) did not share the initial mirroring of the hyetograph. At the onset of ponding, excess rainfall was expended on surface depression storage. It was during this time that the hydrologic connectivity to the outlet was low. At the same time, the hydrologic connectivity of S7 was mainly dictated by the rate of runoff movement in the form of sheet flow over the surface, while more water was retained in depressions upstream. As rainfall progressed, some depressions merged and contributed water to the outlet through their overflow thresholds or pouring points. Accordingly, the hydrologic connectivity increased. After the hydrologic connectivity was complete, the flows between

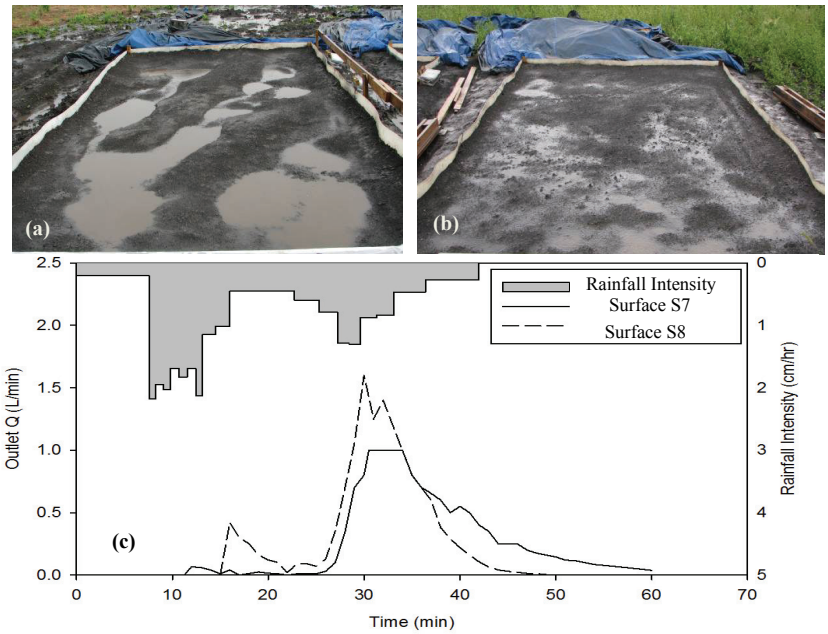

Figure 8. Overland flow experiments for the two field plot surfaces S7 and S8: (a) S7 with ponded water, (b) S8 with ponded water, and (c) hydrographs of S7 and S8.

the rough and smooth field plots (S7 and S8) were similar (fig. 8c). Similar to the hydrograph from S8, the hydrograph of S7 followed the variation of the rainfall intensity (fig. 8c).

It is important to quantify CAs, along with the fractal parameters *D* and *l* to understand some hydrologic processes. At the small scale (first segment), S7 with a smaller *D* is featured with bigger and deeper puddles that are capable of storing more water (fig. 8a). Within each puddle, the elevation change between two points is small at the small spatial scale (i.e., the puddle surface is locally smooth), as quantified by the smaller *l* value (table 3). Thus, water transfers easily within each puddle. At the early stage of rainfall, water infiltrates into the soil and concentrates to the local depressions instead of flowing to the outlet, which delays the initiation of surface runoff (fig. 8c). At this small scale, the effect of surface roughness on overland flow is minimal. In contrast, at the large scale (second segment), S7 is characterized with a greater *D* value and a much higher *l* value (table 3), showing the overall rough surface features (e.g., distribution of puddles). At this large scale, surface topography plays an important role in the overland flow process, since water movement is greatly affected or controlled by the "larger scale" puddles. Surface S8 is characterized with smaller and shallower puddles and a greater number of small CAs than S7 (fig. 8). The difference in overland flow distribution and surface runoff rate between these two surfaces is determined by the overall difference in their topographic conditions. Figure 8c shows the difference in the hydrographs of surfaces S7 and S8. The smooth surface (S8) has a quicker response to rainfall than the rough surface (S7). Due to the high rainfall intensity, the overland flow rate from S8 reaches a peak (about 1.6 L min^{-1}) that is much higher than that of S7 (around 1.0 L min^{-1}). In addition, the rough surface (S7) with a lower *D* value has the potential to retain more water in surface depressions (MDS = 220,457 cm^3), which in turn redistributes surface runoff water, enhances infiltration in the depressions, and delays surface runoff generation. Due to the retention of water in the depressions, the outlet flow reaches a plateau for S7, and the recession part of the hydrograph exhibits a gradual decline, compared with that of S8 (fig. 8c). In contrast, the smooth surface (S8) with a higher *D* value has much smaller depression storage (MDS = 24,676 cm^3), and surface runoff occurs earlier than on surface S7 with a lower *D* value.

In addition, hydrologic processes also show the anisotropic/isotropic properties, which are determined by the anisotropic/isotropic properties of surface microtopography. According to fractal parameters *D* and *l*, the six random rough soil surfaces (S1 to S6) show relatively isotropic properties (fig. 6). For an anisotropic surface, the dominant roughness exists along the directions of lower *D* values. For example, S7 shows anisotropy in *D* at the large scale (second segment) (fig. 7b). The *D* values are small in the directions of 90° to 120° (fig. 7b), along which surface runoff is hindered or blocked by continuously distributed ridges (fig. 8a). For other directions, more puddles can be hydrologically connected (fig. 8a). That is, flow paths may develop more easily along those directions. The puddles on surface S8 are generally small and shallow, and are distributed evenly, resulting in stronger isotropy. Thus, no obvious directional water distribution and runoff process exist (fig. 8b).

From the above analyses, it can be concluded that the spatial complexity of the overland flow processes is highly dependent on the surface topographic conditions. The fractal parameters *D* and *l* are able to provide useful information for understanding the related hydrologic processes. It is of great importance to examine the mechanisms of overland flow generation and other hydrologic processes under the influence of surface microtopography.

SUMMARY AND CONCLUSIONS

In this study, six laboratory surfaces and two field plot surfaces were created, and the semivariogram method was applied for fractal analysis. Particularly, anisotropy/isotropy of surface microtopography was examined for the selected surfaces by directional fractal analysis and was further quantified by introducing a modified anisotropy index. It was demonstrated that directional fractal analysis and the anisotropy index (*a*) were useful for quantifying the anisotropic property of surface microtopography. It was found that surface slope removal had a significant effect on the calculation of fractal parameters. Multifractal analysis was able to capture surface topographic features at different scales. Fractal dimension *D* and crossover length *l* at smaller scales depicted more details on surface microtopography, while the overall topographic features were characterized by *D* and *l* on larger scales. This study showed that *D* had a negative relationship with random roughness (RR) and maximum depression storage (MDS), and a positive relationship with the number of connected areas (NCA). Since surface microtopography affected the distribution of runoff water and the development of the drainage system, the parameters that were able to characterize surface topography (e.g., RR, MDS, NCA, and the fractal parameters *D* and *l*) could be effectively used to improve the understanding of the overland flow generation process. A surface with a smaller *D* value had the potential to retain more water on the surface (in depressions), which in turn redistributed surface water, enhanced infiltration in the depressions, and delayed surface runoff generation. Dominant surface roughness existed along the directions of smaller *D* values. Along those directions, surface runoff was prone to be hindered or blocked by continuously distributed ridges. Other directions possessed better hydrologic connectivity.

ACKNOWLEDGEMENTS

This material is based upon work supported by the National Science Foundation under Grant No. EAR-0907588.

REFERENCES

Abedini, M. J., and M. R. Shaghaghian. 2009. Exploring scaling laws in surface topography. *Chaos, Solitons, and Fractals* 42(4): 2373-2383.

Abedini, M. J., W. T. Dickinson, and R. P. Rudra. 2006. On

depressional storages: The effect of DEM spatial resolution. *J. Hydrol.* 318(1-4): 138-150.
Allmaras, R. R., R. E. Burwell, W. E. Larson, and R. F. Hotl. 1966. Total porosity and random roughness of the interrow zone as influenced by tillage. USDA Conservation Research Report 7. Washington, D.C.: USDA.
Armstrong, A. C. 1986. On the fractal dimensions of some transient soil properties. *European J. Soil Sci*. 37(4): 641-652.
Burrough, P. A. 1983. Multiscale sources of spatial variation in soil. I. The application of fractal concepts to nested levels of soil variations. *J. Soil Sci*. 34(3): 577-597.
Chu, X. 2011. Characterization of microtopography and its hydrologic significance. In *Modeling Hydrologic Effects of Microtopographic Features*, 1-14. X. Wang, ed. Hauppauge, N.Y.: Nova Science Publishers.
Chu, X., J. Zhang, J. Yang, and Y. Chi. 2010. Quantitative evaluation of the relationship between grid spacing of DEMs and surface depression storage. In *Proc. 2010 World Environ. and Water Resources Congress: Challenges of Change*, 4447-4457. R. N. Palmer, ed. Reston, Va.: ASCE.
Chu, X., J. Yang, and Y. Chi. 2012. Quantification of soil random roughness and surface depression storage: Methods, applicability, and limitations. *Trans. ASABE* 55(5): 1699-1710.
Darboux, F., and C. Huang. 2003. An instantaneous-profile laser scanner to measure soil surface microtopography. *SSSA J*. 67(1): 92-99.
Darboux, F., and C. Huang. 2005. Does soil surface roughness increase or decrease water and particle transfers? *SSSA J*. 69(3): 748-756.
Darboux, F., P. Davy, C. Gascuel-Odoux, and C. Huang. 2001. Evolution of soil roughness and flowpath connectivity in overland flow experiments. *Catena* 46(2-3): 125-139.
Eltz, F. L. F., and L. D. Norton. 1997. Surface roughness changes as affected by rainfall erosivity, tillage, and canopy cover. *SSSA J*. 61(6): 1746-1755.
Feder, J. 1988. *Fractals*. New York, N.Y.: Plenum Press.
Gagnon, J.-S., S. Lovejoy, and D. Schertzer. 2006. Multifractal earth topography. *Nonlinear Proc. in Geophysics* 13(5): 541-570.
Govers, G., I. Takken, and K. Helming. 2000. Soil roughness and overland flow. *Agronomy* 20(2): 131-146.
Green, T. R., and R. H. Erskine. 2004. Measurement, scaling, and topographic analyses of spatial crop yield and soil water content. *Hydrol. Proc*. 18(8): 1447-1465.
Hayashi, M., G. Van Der Kamp, and R. Schmidt. 2003. Focused infiltration of snowmelt water in partially frozen soil under small depressions. *J. Hydrol*. 270(3-4): 214-229.
Huang, C. 1998. Quantification of soil microtopography and surface roughness. In *Fractals in Soil Science*, 153-168. P. Baveye, J. Y. Parlange, and B. A. Stewart, eds. Boca Raton, Fla.: CRC Press.
Huang, C., and J. M. Bradford. 1992. Application of a laser scanner to quantify soil microtopography. *SSSA J.* 56(1): 14-21.
Kamphorst, E. C., V. Jetten, J. Guérif, J. Pitkänen, B. V. Iversen, J. T. Douglas, and A. Paz. 2000. Predicting depression storage from soil surface roughness. *SSSA J*. 64(5): 1749-1758.
Klinkenberg, B. 1988. Test of a fractal model of topography. PhD diss. Ontario, Canada: University of Western Ontario, Department of Geography.
Klinkenberg, B., and M. F. Goodchild. 1992. The fractal properties of topography: A comparison of methods. *Earth Surf. Proc. and Landforms* 17(3): 217-234.
Lovejoy, S., D. Lavallée, D. Schertzer, and P. Ladoy. 1995. The *l*1/2 law and multifractal topography: Theory and analysis. *Nonlinear Proc. in Geophysics* 2(1): 16-22.
Mark, D. M., and P. B. Aronson. 1984. Scale-dependent fractal dimensions of topographic surfaces: An empirical investigation, with applications in geomorphology and computer mapping. *Math. Geology* 16(7): 671-683.
Martin, Y., C. Valeo, and M. Tait. 2008. Centimetre-scale digital representations of terrain and impacts on depression storage and runoff. *Catena* 75(2): 223-233.
McClean, C. J., and I. S. Evans. 2000. Apparent fractal dimensions from continental-scale digital elevation models using semivariogram methods. *Trans. in GIS* 4(4): 361-378.
Moore, I. D., and C. L. Larson. 1979. Estimating micro-relief surface storage from point data. *Trans. ASAE* 22(5): 1073-1077.
O'Callaghan, J. F., and D. M. Mark. 1984. The extraction of drainage networks from digital elevation data. *Computer Vision, Graphics, and Image Proc.* 28(3): 323-344.
Onstad, C. A. 1984. Depression storage on tilled soil surfaces. *Trans. ASAE* 27(3): 729-732.
Perfect, E., and B. D. Kay. 1995. Applications of fractals in soil and tillage research: A review. *Soil and Tillage Res*. 36(1-2): 1-20.
Quattrochi, D. A., N. S.-N. Lam, H. L. Qiu, and W. Zhao. 1997. Image characterization and modeling systems (ICAMS): A geographic information system for the characterization and modeling of multiscale remote-sensing data. In *Scale in Remote Sensing and GIS*, 295-307. D. A. Quattrochi and M. Goodchild, eds. Boca Raton, Fla.: CRC Press.
Sun, W., G. Xu, P. Gong, and S. Liang. 2006. Fractal analysis of remotely sensed images: A review of methods and applications. *Intl. J. Remote Sensing* 27(22): 4963-4990.
Sung, Q. C., Y. C. Chen, and P. C. Chao. 1998. Spatial variation of fractal parameters and its geological implications. *Tao* 9(4): 655-672.
Vázquez, E. V., J. G. V. Miranda, and A. P. González. 2005. Characterizing anisotropy and heterogeneity of soil surface microtopography using fractal models. *Ecol. Modeling* 182(3-4): 337-353.
Vázquez, E. V., J. G. V. Miranda, and A. P. González. 2007. Describing soil surface microrelief by crossover length and fractal dimension. *Nonlinear Proc. in Geophysics* 14(3): 223-235.
Vázquez, E. V., S. R. Vieira, I. C. De Maria, and A. P. González. 2010. Fractal dimension and geostatistical parameters for soil microrelief as a function of cumulative precipitation. *Scientia Agricola* 67(1): 78-83.
Western, A. W., G. Blöschl, and R. B. Grayson. 2001. Toward capturing hydrologically significant connectivity in spatial patterns. *Water Resources Res*. 37(1): 83-97.
Xia, Z. G. 1993. The use and limitations of fractal geometry in digital terrain modeling. PhD diss. New York, N.Y.: City University of New York, Department of Geology and Geography.
Yokoya, N., K. Yamamoto, and N. Funakubo. 1989. Fractal-based analysis and interpolation of 3D natural surface shapes and their application to terrain modeling. *Computer Vision, Graphics, and Image Proc.* 46(3): 284-302.
Zribi, M., V. Ciarletti, O. Taconet, J. Paille, and P. Boissard. 2000. Characterization of the soil structure and microwave backscattering based on numerical three-dimensional surface representation: Analysis with a fractional Brownian model. *Remote Sensing of Environ*. 72(2): 159-169.